

A Conservative Surface Tension Operator for Compressible Flows within Stiff Media

By **B. Hejazialhosseini**[†], **X. Y. Hu**, **N. A. Adams** AND **P. Koumoutsakos**[†]

Lehrstuhl für Aerodynamik und Strömungsmechanik, Technische Universität München
Boltzmannstr. 15, 85748 Garching b. München

We present a multiphase compressible flow solver that accounts for surface tension and is capable of handling stiff media. The solver enjoys recent developments on oscillation-free modeling of compressible flows using finite volume discretization when stiffened equation of state is used. Surface tension is applied through a conservative form based on the projection of one of the advected fluid properties of the solver. We employ fifth order WENO reconstructions along with HLL numerical flux as the approximate Riemann solver. Advection equation of material properties is cast into a conservative form to be unified with the flux-based hyperbolic solver and an extra modification is made based on the advection equations to be consistent with the HLL flux. The solver is applied to the severe case of oscillating ellipsoidal droplet of water in air as well as the rising bubble problem. We also explain why levelset-based advection of interface together with stiffened equation of state cannot guarantee a stable solution.

1. Introduction

Continuum modeling and simulation of multicomponent flows has applications in cavitation and bubble collapse in lithotripsy, atomization in sprays, inertial confinement fusion and so on. In many practical situations, compressibility effects cannot be neglected. Moreover, when the interface between the phases undergo large and complex deformations, capillary effects can become equally important as the convection, if not dominant.

Different approaches to deal with multiphase flows under capillary effects have been presented in [1, 2]. The former uses a combined levelset/volume-of-fluid method in the context of incompressible flows while the later employs discontinuous Galerkin ALE formulation for front tracking and the hyperbolic system of equations and a non-conservative form of the capillary force. However [2] does not consider any stiff media present in the considered flows and [1] explicitly solves for the pressure.

In a compressible flow setting, stiff media is often represented by stiffened equation of state [3] and oscillation-free treatment of the governing system of equations has only recently been demonstrated [4]. Surface tension is often modeled as a force term after [5] which requires a definition for the normal and the curvature of the interface. This in turn translates into numerical differentiation of the conventional interface markers such as volume fraction or levelset twice.

In case of a levelset-based advection, distortions are inevitable due to complex flow maps and re-distancing is necessary to ensure accurate calculation of interface normals and curvature. Different re-distancing procedures have been suggested to ensure that

[†] Chair of Computational Science, ETH Zurich, Switzerland

the interface location does not change [6] but in general, since material properties such as specific heat ratios need to be computed based on the levelset field, these methods do not preserve cell averages of energy over the smooth interfaces.

In this work we use a conservative form of the surface tension together with the recent developments in simulation of multiphase compressible flows within stiff media. The feasibility of such a solver is examined in the problem of an oscillating droplet of water in air and to the problem of a rising bubble of air inside a stiff medium. Finally we briefly discuss the reason for inability of levelset-based solvers in simulating multiphase compressible flows when stiff media are involved.

2. Governing equations

We consider an inviscid compressible flow described by the Euler equations as a one-fluid model [7] for two phase flows:

$$\begin{aligned}\frac{\partial \rho}{\partial t} + \nabla \cdot (\rho \mathbf{u}) &= 0 \\ \frac{\partial(\rho \mathbf{u})}{\partial t} + \nabla \cdot (\rho \mathbf{u} \otimes \mathbf{u} + p \mathbf{I}) &= \mathbf{0} \\ \frac{\partial(E)}{\partial t} + \nabla \cdot ((E + p)\mathbf{u}) &= 0\end{aligned}\quad (2.1)$$

with ρ being the density, \mathbf{u} the velocity vector, p the pressure and E the total energy.

We model the behavior of both phases through a stiffened equation of state [3] of the form:

$$\Gamma p + \Pi_\infty = E - \frac{1}{2} \rho |\mathbf{u}|^2 \quad (2.2)$$

with $\Gamma = 1/(\gamma - 1)$ and $\Pi_\infty = \gamma p_\infty/(\gamma - 1)$ where γ is the mixture ratio of specific heats and p_∞ is the mixture correction pressure. The mixture properties are defined by:

$$\begin{aligned}\gamma &= 1 + \frac{(\gamma_2 - 1)(\gamma_1 - 1)}{\phi(\gamma_1 - 1) + (1 - \phi)(\gamma_2 - 1)} \\ p_\infty &= \frac{\gamma - 1}{\gamma} \left(\frac{\gamma_1 p_{\infty_1} (1 - \phi)}{\gamma_1 - 1} + \frac{\gamma_2 p_{\infty_2} \phi}{\gamma_2 - 1} \right)\end{aligned}\quad (2.3)$$

where ϕ specifies the initial color function separating the two phases.

To complete the model for two phase compressible flows, two advection equations of the form:

$$\begin{aligned}\frac{\partial \Gamma}{\partial t} + \mathbf{u} \cdot \nabla \Gamma &= 0 \\ \frac{\partial \Pi_\infty}{\partial t} + \mathbf{u} \cdot \nabla \Pi_\infty &= 0\end{aligned}\quad (2.4)$$

are introduced for the material properties of the phases.

Surface tension is often modeled as a distributed body force (CSF, introduced in [5] which is applied to a band close to the interface. In this work, we employ another approach in which capillary effects are modeled via a conservative operator. The conventional surface tension force can be written as:

$$\mathbf{F}_\sigma|_{\phi=0} = \sigma \kappa \mathbf{n} \quad (2.5)$$

with κ being the mean curvature, \mathbf{n} the normal of the interface and σ the surface tension

coefficient. One can rewrite the surface force as:

$$\begin{aligned}\mathbf{F} &= \nabla \cdot \mathbf{T} \\ \mathbf{T} &= \sigma(\mathbf{I} - \mathbf{n}^T \mathbf{n}) |\nabla C|\end{aligned}\quad (2.6)$$

where C is a color function describing the two phase interface. After [8, 9] the surface tension tensor, \mathbf{T} , can be put into the form:

$$\mathbf{T} = \sigma \left(\frac{1}{d} \mathbf{I} - \mathbf{n}^T \mathbf{n} \right) |\nabla C|. \quad (2.7)$$

where d is the dimension of the problem. As noted by [10], the direct computation of \mathbf{n} can be replaced by the following:

$$\mathbf{T} = \sigma \frac{1}{|\nabla C|} \left(\frac{1}{d} \mathbf{I} |\nabla C|^2 - \nabla C^T \nabla C \right). \quad (2.8)$$

The final system of equations without considering viscous effects reads:

$$\begin{aligned}\frac{\partial \rho}{\partial t} + \nabla \cdot (\rho \mathbf{u}) &= 0 \\ \frac{\partial (\rho \mathbf{u})}{\partial t} + \nabla \cdot (\rho \mathbf{u} \otimes \mathbf{u} + p \mathbf{I} + \mathbf{T}) &= \mathbf{0} \\ \frac{\partial (E)}{\partial t} + \nabla \cdot ((E + p) \mathbf{u} + \mathbf{T} \cdot \mathbf{u}) &= 0.\end{aligned}\quad (2.9)$$

which along with the advection equations forms a quasi-conservative system.

3. Numerical method

3.1. Hyperbolic solver

The hyperbolic part of the governing equations (2.9) can be cast into the vector form:

$$\mathbf{q}_t + \nabla \cdot \mathbf{f}(\mathbf{q}) = \mathbf{0} \quad (3.1)$$

where $\mathbf{q}(x, t) = (\rho, \rho \mathbf{u}, E)^T$, with initial conditions $\mathbf{q}(x, 0) = \mathbf{q}_0(x)$ and appropriate boundary conditions. The integral form of (3.1), written in 1D as:

$$\oint (\mathbf{q} dx - \mathbf{f}(\mathbf{q}) dt) = 0 \quad (3.2)$$

is used as a starting point for the finite volume discretization. If the computational domain is uniformly discretized by finite volumes, then cell averages of $\{\mathbf{q}_i\}$ at time $t = t_n$ and the flux:

$$\mathbf{F}_{i\pm 1/2} = \frac{1}{\Delta t} \int_{t_n}^{t_{n+1}} \mathbf{f}(\mathbf{q}_{i\pm 1/2}(t)) dt, \quad (3.3)$$

determine the new solution at time $t_{n+1} = t_n + \Delta t$, \mathbf{q}^{n+1} . In order to avoid the expensive Riemann solver [11], $\mathbf{F}_{i\pm 1/2}$ is approximated by a numerical flux $\hat{\mathbf{F}}_{i\pm 1/2}^n$. The new values of $\{\mathbf{q}_i^{n+1}\}$ are found after one simulation step, by evaluating the numerical fluxes and perform a time integration for all the averages:

$$\mathbf{q}_i^{n+1} = \mathbf{q}_i^n - \frac{\Delta t}{\Delta x} (\hat{\mathbf{F}}_{i+1/2}^n - \hat{\mathbf{F}}_{i-1/2}^n). \quad (3.4)$$

Since $\hat{\mathbf{F}}_{i+1/2}^n$ and $\hat{\mathbf{F}}_{i-1/2}^n$ depend on the local cell neighbors of \mathbf{q}_i^n , the simulation step formulated in (3.4) can be seen as a non-linear uniform filtering at the location of \mathbf{q}_i^n .

There have been various formulations for these numerical fluxes namely Roe [12], Lax-Friedrichs [13] and HLL [14]. In this paper, we use the HLLC [15] flux which is capable of correctly resolving isolated shocks and rarefaction waves.

The exact Riemann solver and its approximate versions require a reconstruction step which provides them with the left and the right states as well as the exact and approximate characteristic velocities on the cell interfaces. A broad range of reconstruction-evolution methods has been developed to make this reconstruction high order as well as oscillation-free e.g. TVD/MUSCL [16], PPM [17], ENO [18], etc.

Besides, it has also been shown that the reconstruction of conserved quantities, \mathbf{q} , leads to oscillations in the pressure close to the contact discontinuity and violates the zero jump conditions of velocity and pressure across the interface generating spurious wiggles on the interface [19]. This can be overcome by reconstructing the primitive quantities $\mathbf{u} = (\rho, u, v, w, p)$, based on which the conserved quantities and fluxes are then calculated [20, 21]. We use fifth order WENO scheme [22, 23] to this end. Total Variation Diminishing (TVD) low-storage Runge-Kutta scheme of order three is used as the time-stepper [24].

Moreover, as demonstrated by [4, 19], not every function is suitable to advect in order to retrieve the material properties: to avoid spurious oscillations in the pressure field, $1/(\gamma - 1)$ and $\gamma p_\infty/(\gamma - 1)$ should be advected using the same Riemann solver as for the conservation equations. Therefore a modified form of the advection equation:

$$\frac{\partial \phi}{\partial t} + \nabla \cdot (\phi \mathbf{u}) = \phi \nabla \cdot \mathbf{u} \quad (3.5)$$

is used for the treatment of advected material properties. In order to compute $\nabla \cdot \mathbf{u}$ in the right hand side of equation (3.5) on the finite volume cell i , one needs to select correct velocities on the cell interfaces located at $x_{i\pm 1/2}$. We therefore adopt a similar idea as in [19, 20] to calculate the velocities on the cell boundaries and for a hyperbolic solver based on HLLC flux, one can write:

$$u_{i\pm 1/2} = \frac{a_{i\pm 1/2}^+ u_{i\pm 1/2}^- + a_{i\pm 1/2}^- u_{i\pm 1/2}^+}{a_{i\pm 1/2}^+ - a_{i\pm 1/2}^-} \quad (3.6)$$

where u^\pm denotes the reconstructed left and right velocities at the cell interface and a^\pm are the reconstructed left and right-running characteristic speeds. The term ϕ on the right hand side of (3.5) can be obtained via a mid-point quadrature and therefore together with Eq. (3.6) approximates the right hand side to the second order. It should be mentioned that, as shown in [4], when temperature directly comes into the flow calculations, an advection equation for volume fraction needs to be added to the system of equations in order to prevent oscillations in temperature. However this is not the case in the present work.

3.2. Surface tension operator

We normalize one of the material properties, here Γ , to obtain a color function (or a volume fraction), which is used as C in Eq. (2.8). The values of C are in turn used to compute $|\nabla C|$ and the surface tension tensor \mathbf{T} on the cell interfaces to the second order. In 3D, we use the information of 3^3 cells to compute the central differences and averages necessary for the surface tension tensor on cell boundaries. We consider a fixed surface tension coefficient in this work, however the conservative form of the capillary forces supports varying σ on the interface.

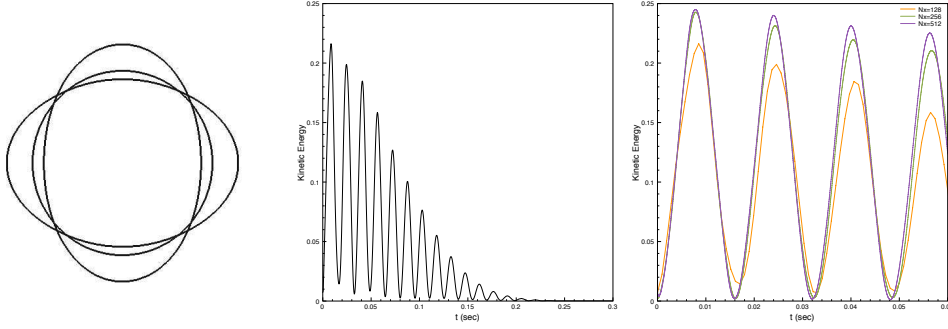


FIGURE 1. Interface of the droplet (left), temporal evolution of the global kinetic energy for the oscillating droplet (middle), grid convergence of the global kinetic energy (right).

4. Results

4.1. Oscillating droplet

In this test case, an ellipsoidal droplet of water, modeled by $\gamma = 2.4$ and $p_\infty = 10^7 Pa$, is placed inside air, modeled by $\gamma = 1.4$ and $p_\infty = 0 Pa$. The ellipsoid is initially defined by $(x - 0.5)^2/0.1^2 + (y - 0.5)^2/0.06^2 = 1$. The initial density is set to $100 kg/m^3$ for the droplet and to $1 kg/m^3$ for the surrounding air. The ambient pressure is set to $10^5 Pa$. The computational domain is $[0, 1]^2$ and we use zeroth order extrapolation for the non-reflecting boundaries. Surface tension coefficient is set to $341.64 N/m$ deduced from a similar test in [8]. The computational domain is $[0, 1]^2$ and the CFL number is fixed at 0.6.

We plot the evolution of the kinetic energy in Fig. 1 (left). The period of the oscillations in the kinetic energy of the field, measured from the plot, is found to be about 0.02951 seconds. Analytical period of oscillation for this problem after [25] can be calculated from:

$$\omega = (o^3 - o) \frac{\sigma}{(\rho_l + \rho_g)R^3} \quad (4.1)$$

which for our problem, using the equilibrium radius of $0.0734 m$ and the oscillation mode $o = 2$, is 0.02785 seconds. We show the grid convergence of the global kinetic energy for grid sizes of 128^2 , 256^2 and 512^2 in Fig. 1 (right).

4.2. Rising bubble

In this test case, we simulate the behavior of an air bubble rising in water, modeled by $\gamma = 2.1$ and $p_\infty = 2 \cdot 10^5$. The density ratio between the surrounding and the bubble is set to 100. The ambient pressure is set to 1000. The non-dimensional number which characterizes this flow is the Eotvos number defined by:

$$Eo = \frac{\Delta \rho g l^2}{\sigma} \quad (4.2)$$

and for the two test cases studied here is chosen to be 1.3 and $1.3 \cdot 10^2$. Initial shape of the bubble is chosen to be an ellipsoid as in Sec. 4.1. The computational domain is set to $[0, 1] \times [0, 3]$ and is discretized by 128×384 elements which results in 20 grid points per equilibrium radius.

In Fig. 2, we present the air/water interface for the rising bubble flow. At $Eo = 1.3 \cdot 10^2$, the flow is very much dominated by convective forces due to gravity and the bubble undergoes a large acceleration in the middle compared to the sides and therefore it

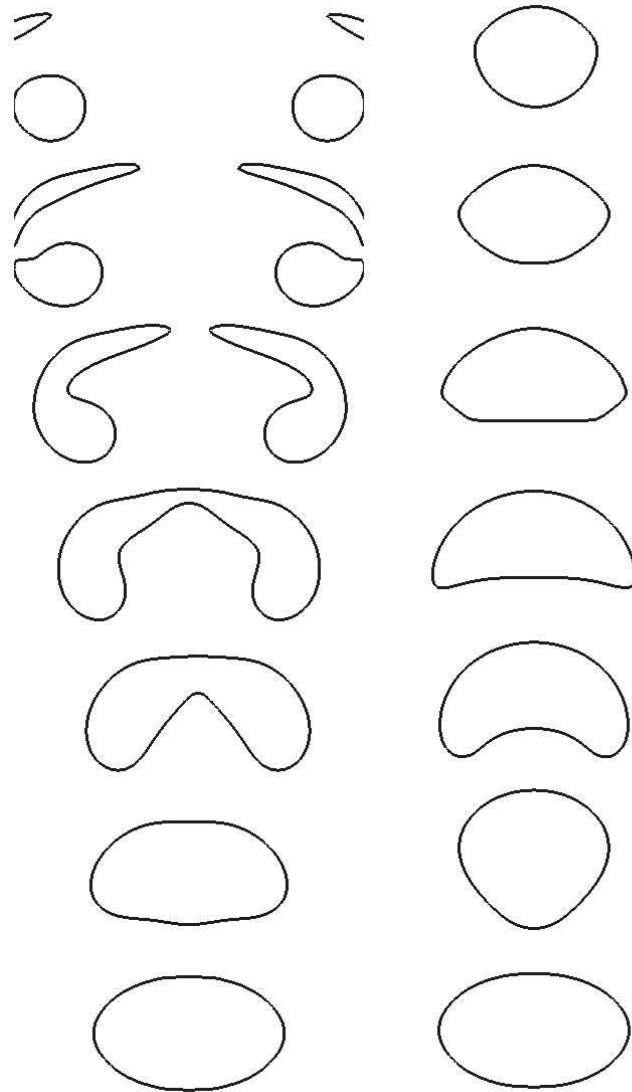


FIGURE 2. Interface ($\alpha = 0.5$) of the rising bubble test case at $t = 0, 0.15, 0.28, 0.36, 0.57, 0.71$ and 1.00 (from bottom to top) for $Eo = 1.3 \cdot 10^2$ (left) 1.3 (right).

breaks apart. At $Eo = 1.3$, capillary effects seem to become significant and therefore the ellipsoidal bubble is closer to its equilibrium circular shape at the top end of the domain. These observations are in agreement with the experimental bubble dynamics map in [8].

4.3. Inability of levelset formulation for the advection of multiphase interfaces in stiff media

Levelset-based advection of interfaces is another common approach in the field of multiphase flows. In compressible flows, one needs to filter the levelset field with a Heaviside function to retrieve material properties such as the specific heat ratio or the correction

pressure for the stiffness of the media. Using a sharp Heaviside or one with a fixed smoothing length (often fixed at the maximum resolution) is not in general consistent with the hyperbolic solver as numerical fluxes normally tend to smoothen out isolated contact discontinuities even when there is no velocity in the flow. Therefore computed pressure over the smoothened interface will be different than what is implied by the numerical flux machinery. This problem becomes severe when dealing with realistic correction pressures (up to 10^3 times more than the ambient pressure) as the computed pressure based on the filtered levelset, introduces a large amount of internal energy on one side of the interface. In this regard, advection of material properties (or a function of properties as shown in this work) is favored over the use of levelset function.

5. Conclusions

We have shown that the recent advances in treatment of multiphase compressible flows within stiff media can be successfully employed together with a conservative surface tension operator computed based on one of the advected material properties. We have also discussed about why levelset-based advection and re-distancing can fail in the considered flows. Further improvements can be made to ensure the mass conservation of the individual phases by introducing an extra advection equation for the volume fraction of one of the phases. This can also remove the extra normalization step in the current solver for computing surface normals. Future work involves introducing the Brinkmann penalization model [26] to support solid obstacles within the solver.

Acknowledgments

Financial support has been provided by the German Research Foundation (Deutsche Forschungsgemeinschaft – DFG) in the framework of the Sonderforschungsbereich Transregio 40 and the IGSSE (International Graduate School of Science and Engineering) at Technische Universität München. Computational resources have generously been provided by the Leibniz-Rechenzentrum München (LRZ).

References

- [1] BRACKBILL, J. U., KOTHE, D. B. AND ZEMACH, C. (1994). A Level Set Approach for Computing Solutions To Incompressible 2-Phase Flow. *J. Comp. Phys.*, **114**, 146–159.
- [2] NGUYEN, V., PERAIRE, J., KHOO, B. C. AND PERSSON, P. (2010). A discontinuous Galerkin front tracking method for two-phase flows with surface tension. *Computers and Fluids*, **39**, 1–14.
- [3] HARLOW, F. AND AMSDEN, A. (1971). Fluid dynamics. *LANL Monograph LA-4700*.
- [4] JOHNSEN, E., HAM, F. AND LARSSON, J. (2009). Numerical errors generated by shock-capturing schemes in compressible multicomponent flows. *Center for Turbulence Research – Annual Research Briefs 2009*.
- [5] SUSSMAN, M., SMEREKA, P. AND OSHER, S. (1992). A continuum method for modeling surface-tension. *J. Comp. Phys.*, **100**, 335–354.
- [6] RUSSO, G. AND SMEREKA, P. (2000). A remark on computing distance functions. *J. Comp. Phys.*, **163**, 51–67.

- [7] PROSPERETTI, A. AND TRYGGVASON, G. (2008). *Computational Methods for Multiphase Flow*. Cambridge University Press.
- [8] PERIGAUD, G. AND SAUREL, R. (2005). A compressible flow model with capillary effects. *J. Comp. Phys.*, **209**, 139–178.
- [9] HU, X. Y. AND ADAMS, N. A. (2006). A multi-phase SPH method for macroscopic and mesoscopic flows. *J. Comp. Phys.*, **213**, 844–861.
- [10] WU, J., YU, S. T. AND JIANG, B. N. (1998). Surface tension and viscosity with lagrangian hydrodynamics on a triangular mesh. *International Journal for Numerical Methods in Engineering*, **42**, 583–600.
- [11] TORO, E. F. (1999). *Riemann Solvers and Numerical Methods for Fluid Dynamics*. Springer-Verlag, Berlin.
- [12] ROE, P. L. (1981). Approximate Riemann solvers, parameter vectors and difference-schemes. *J. Comp. Phys.*, **43**, 357–372.
- [13] ROE, P. L. (1954). Weak solutions of nonlinear hyperbolic equations and their numerical computation. *Communication on Pure and Applied Mathematics*, **7**, 159–193.
- [14] HARTEN, A., LAX, P. D. AND VAN LEER, B. (1983). On upstream differencing and Godunov-type schemes for hyperbolic conservation laws. *SIAM Review*, **25**, 35–61.
- [15] EINFELDT, B. (1988). Uniformly high order accurate essentially non-oscillatory schemes 3. *SIAM journal on numerical analysis*, **25**, 294–318.
- [16] ANDERSON, W. K., THOMAS, J. L. AND VAN LEER, B. (1986). Comparison Of Finite Volume Flux Vector Splittings For The Euler Equations. *AIAA Journal*, **24**, 1453–1460.
- [17] COLELLA, P. AND WOODWARD, P. R. (1984). The Piecewise Parabolic Method (PPM) For Gas-Dynamical Simulations. *J. Comp. Phys.*, **54**, 174–201.
- [18] HARTEN, A., ENGQUIST, B., OSHER, S. AND CHAKRAVARTHY, S. R. (1997). Uniformly high order accurate essentially non-oscillatory schemes 3. *J. Comp. Phys.*, **131**, 3–47.
- [19] SAUREL, R. AND ABGRALL, R. (1999). A simple method for compressible multi-fluid flows. *SIAM Journal on Scientific Computing*, **21**, 1115–1145.
- [20] JOHNSEN, E. AND COLONIUS, T. (2006). Implementation of WENO schemes in compressible multicomponent flow problems. *J. Comp. Phys.*, **219**, 715–732.
- [21] MIGNONE, A., PLEWA, T. AND BODO, G. (2005). The piecewise parabolic method for multidimensional relativistic fluid dynamics. *Astrophysical Journal Supplement Series*, **160**, 199–219.
- [22] LIU, X. D., OSHER, S. AND CHAN, T. (1994). Weighted Essentially Nonoscillatory Schemes. *J. Comp. Phys.*, **115**, 200–212.
- [23] JIANG, G. S. AND SHU, C. W. (1996). Efficient implementation of weighted ENO schemes. *J. Comp. Phys.*, **126**, 202–228.
- [24] WILLIAMSON, J. H. (1980). Low-Storage Runge-Kutta Schemes. *J. Comp. Phys.*, **35**, 48–56.
- [25] FYFE, D. E., ORAN, E. S. AND FRITTS, M. J. (1988). Surface tension and viscosity with lagrangian hydrodynamics on a triangular mesh. *J. Comp. Phys.*, **76**, 349–384.
- [26] LIU, Q. AND VASILYEV, O. V. (2007). A Brinkman penalization method for compressible flows in complex geometries. *J. Comp. Phys.*, **227**, 946–966.